Physica B 666 (2023) 415132

Contents lists available at ScienceDirect

Physica B: Condensed Matter

journal homepage: www.elsevier.com/locate/physb

Ground state structural, lattice dynamic, thermodynamic and optical properties of the Ba_2CaMoO_6 ordered perovskite

C.E. Deluque Toro [a], V.E. Vergara [a], A.V. Gil Rebaza [b], D.A. Landínez Téllez [c,d], J. Roa-Rojas [c,*]

[a] Grupo de Nuevos Materiales, Facultad de Ingeniería, Universidad del Magdalena, Santa Marta, Colombia
[b] Dpto. de Física, Facultad de Ciencias Exactas, Universidad Nacional de La Plata – UNLP, Instituto de Física La Plata IFLP, CONICET-CCT La Plata13 (1900), La Plata, Argentina
[c] Grupo de Física de Nuevos Materiales, Departamento de Física, Universidad Nacional de Colombia, 111321, Bogotá DC, Colombia
[d] Grupo de Estudios de Materiales GEMA, Departamento de Física, Universidad Nacional de Colombia, 111321, Bogotá DC, Colombia

ARTICLE INFO

Keywords:
Perovskite material
Structure
Optical and thermodynamical features

ABSTRACT

Ab-initio calculations based on density functional theory have been performed to establish the ground state properties for the double perovskite type material Ba_2CaMoO_6. The calculations were carried out through the Projector Augmented Wave Method and the exchange and correlation was described using the Perdew-Burke-Ernzerhof parameterization of the Generalized Gradient Approximation. The study included structural analysis of the material, as well as thermodynamic, cell dynamics and optical properties at its transition between the tetragonal *I4/m* and cubic Fm $\bar{3}$ m phases. The results on the structural stability reveal that the phase with space group of *I4/m* is more stable. Likewise, the structural phase transition was obtained for a pressure of 0.067 GPa. On the other hand, the analysis of the electronic properties shows that the material presents a semiconducting behaviour, with a direct band gap of 2.40 eV and 2.26 eV for the tetragonal and cubic structures, respectively. In addition to agreeing with the experimental values reported in the literature, the results suggest possibilities for the application of this material in photodetectors, light emitters and devices for power electronics. © 2023 Elsevier Science. All rights reserved.

1. Introduction

For many years, perovskite-type materials have been extensively studied because of the diversity of physical properties they exhibit that can be tuned from variations in their chemical composition. Their generic formula is ABX_3, where A can be an earthy alkali or rare earth, and sometimes a semi-metal, B is usually a transition metal or rare earth and X a halogen but is usually oxygen when the material is a perovskite-type oxide such as that which will be considered in the present paper, so the formula is modified to ABO_3 [1]. The stability of the unit cell depends on several factors, among them the ionic radius of the cations A and B, being likely the synthesis of those compounds where these radii comply with $r_A > r_B$, where *r* represents the ionic radius of the cation. As long as the crystallographic stability of the unit cell, given by the global instability index [2], is maintained, it is possible to introduce stoichiometric modifications such as the one that gives rise to the so-called double perovskite. In this, the B cation is substituted by 50% by another B′, so that the generic formula takes the form $AB_{0.5}B'_{0.5}O_3$, with the particularity that the B and B′ cations usually adopt an intercalated arrangement along the crystallographic axes, forming what is called a salt rock superstructure. Thus, its formula is usually written as $A_2BB'O_6$ [3]. The presence of the B′ cation includes a new degree of freedom in the search for new physical properties, which has allowed obtaining double perovskites that show superconductivity [4], high conductivity [5], halfmetallicity [6,7], coexistence of ferromagnetism and semiconductivity [8–10], multiferroicity [11], among other properties with applicability in spintronics technology [12].

Among the recently investigated double perovskite-type materials, Ba_2CaMoO_6 is particularly interesting because the A and B sites of the unit cell are occupied by earthy alkali. Meanwhile, the ionic radius of Sr in its cuboctahedral coordination is 1.44 Å while the ionic radius of Ca in its octahedral coordination is 1.00 Å. This large difference between the sizes of the cations is a first factor towards the structural stability of the material. On the other hand, the so-called tolerance factor, defined as [10].

* Corresponding author.
E-mail address: jroar@unal.edu.co (J. Roa-Rojas).

https://doi.org/10.1016/j.physb.2023.415132
Received 9 April 2023; Received in revised form 30 June 2023; Accepted 12 July 2023
Available online 13 July 2023
0921-4526/© 2023 The Authors. Published by Elsevier B.V. This is an open access article under the CC BY license (http://creativecommons.org/licenses/by/4.0/).

$$\tau = \frac{\sqrt{2}(r_{Ba} + r_O)}{(r_{Ca} + r_{Mo} + 2r_O)} \quad (1)$$

where r_{Ba}, r_{Ca} and r_{Mo} are the ionic radii of the Ba, Ca and Mo cations and r_O represents the ionic radius of the anion O, yields a value $\tau = 0.9740$, whose proximity to the ideal value $\tau = 1$ gives it a high probability of synthesis in the laboratory. Finally, the so-called global instability index, is given by the root-mean-square deviation of the experimental bond valence sums from the atomic valence [13]

$$GII = \sqrt{\frac{\sum_{i=1}^{N} (d_i)^2}{N}} \quad (2)$$

where N is the number of ions and d is the bond discrepancy factor defined as the deviation of the bond valence sum from the formal valence [14]. For Ba_2CaMoO_6 a value GII = 0.03366 is obtained. Predictions for perovskite-type materials suggest that GII values > 0.2 have a low probability of synthesis [2], which allows us to assume that the GII value found is related to good structural stability.

A first report on the Ba_2CaMoO_6 material corresponds to a theoretical and experimental work in which its semiconductor character with a bandgap E_g = 2.7 eV was established [15]. Subsequently, absorption coefficient calculations were carried out, assuming a cubic space group, Fm $\overline{3}$ m, determining the bandgap as E_g = 2.6 eV [16]. Recently the material was synthesized, showing crystallization in a cubic structure, space group Fm $\overline{3}$ m and evidencing a structural transition at T = 200 K to a tetragonal crystallographic phase, space group *I4/m* [17]. In the same report, this transition was corroborated through specific heat and differential scanning calorimetry (DSC) and synchrotron X-ray diffraction (XRD) measurements. Theoretical calculations, considering a cubic structure, show that the partial inclusion of Nb in the crystallographic sites of Mo promotes the stability of ferromagnetic interactions in a half-metallic state [18]. Meanwhile, from the experimental and theoretical reports concerning this material, the structural dependence under the application of temperature and pressure gradients is still a controversial issue. The aim of the present work is to carry out a complete theoretical study of the electronic and optical properties of the Ba_2CaMoO_6 material, in order to establish the stability of the structural phase in the fundamental state and its behaviour under the application of finite temperatures and pressures. The results reveal that at low temperatures the most stable phase is of the tetragonal type. However, both the tetragonal and cubic phases exhibit optical properties applicable in optoelectronic devices.

2. Calculation method

In order to establish the structural ground state and their respective thermodynamic and optical properties for the double perovskite Ba_2CaMoO_6, several ab-initio calculations have been performed in the framework of Density Functional Theory (DFT). The starting point was the self-consistent Kohn-Sham equations, which were solved through the Pseudopotential and Plane Wave Method that is implemented in the Vienna Ab-initio Simulation Package (VASP) [19]. All calculations were performed using a 520 eV cut-off energy, describing the irreducible Brilloiun zone of the reciprocal space by a dense mesh-grid of 13x13x13 and 13x13x9 k-points in the Monkhorst-Pack scheme for the cubic and tetragonal structures, respectively [20]. The Perdew-Burke-Ernzerhof parameterization of the Generalized Gradient Approximation (GGA-PBE) was carried out to include the exchange-correlation potential by means of an accurate description of the electronic structure and optical properties of the material [21]. For this purpose, a Hubbard potential correction (GGA + U), with a value U = 4.38 eV for the d-Mo orbital, was considered. The atomic positions and lattice parameters were optimized until the interatomic forces and the Pulay stress were less than 0.001 eV/A and 0.1 kB, respectively. The dynamical calculations of the lattice were computed using the frozen phonon method, as implemented in the Phonopy code [22]. For this purpose, a 2 × 2 × 2 supercell was considered. Additionally, the quasi-harmonic approach was used for the calculation of thermophysical properties, such as Gibb's energy and specific heat at constant volume [23].

3. Results and discussion

3.1. Structural properties

From the experimental reports mentioned and cited in the introduction for the Ba_2CaMoO_6 double perovskite, total energy minimization processes as a function of unit cell volume were performed and fitted to the Murnaghan equation of state [24], considering the tetragonal *I4/m* and cubic Fm $\overline{3}$ m structures. Using the parameters obtained in the process, which are shown in Table 1, the structures exemplified in Fig. 1 were built. Meanwhile, it is important to note that the lowest energy corresponded to the tetragonal structure, with E = 0.065 eV with respect to the cubic structure.

Both the energy minimization and the GII calculation are important because they represent additional criteria to the tolerance factor for establishing the most probable crystallization structure of the material, since the value of τ is the same for the two structures studied. In Table 1, Wyckoff's letters *a, b, c, e* and *h* determine all points for which the site-symmetry groups are conjugate subgroups of the respective Fm $\overline{3}$ m and *I4/m* space groups, on a case-by-case basis. The position of oxygen for the cubic case corresponds with the position of O_1 in square base of the tetragonal structure, suggesting that, as the cell is stretched along the crystallographic axis *c* to adopt the latter structure, the major distortions are accounted for by the bonds between Ba cations and oxygen anions. This can be corroborated in Table 1, noting that the Ca–O and Mo–O interatomic distances related to the CaO_6 and MoO_6 octahedra are the same for both the cubic and tetragonal cells.

The position of oxygen for the cubic case corresponds with the position of O_1 in square base of the tetragonal structure, suggesting that, as the cell is stretched along the crystallographic axis *c* to adopt the latter structure. Although between the two structures there is no change in the dimensions of the octahedra, a major difference has to do with the octahedral distortion that takes place along the crystallographic axis *c*, which is observed in the occurrence of tilt angles of 9.395° and 11.723° for the CaO_6 and MoO_6 octahedra, respectively. Finally, the distorting

Table 1
Structural parameters calculated for the probable cubic and tetragonal structures of the Ba_2CaMoO_6 material.

Cubic Structure; Fm $\overline{3}$ m space group; Glazer Notation *ååå*; *a* = 5.4966 Å; τ = 0.9740; GII = 0.218135

Wyckoff Position	*x*	*y*	*z*	Interatomic distances (Å)	
Ba-8c	0.2500	0.2500	0.2500	Ba(8c)-O(24e)	3.0357
Ca-4a	0.0000	0.0000	0.0000	Ca(4a)-O(24e)	2.3735
Mo-4b	0.5000	0.0000	0.0000	Mo(4b)-O(24e)	1.9070
O-24e	0.2772	0.0000	0.0000	Bond angles Ca–*O*–Mo: 180.0°	

Tetragonal Structure; *I4/m* space group; Glazer Notation *ååc̄*; *a* = 5.9890 Å, *c* = 8.5430 Å; τ = 0.9740; GII = 0.033655

Wyckoff Position	***x***	***y***	***z***	**Interatomic distances (Å)**	
Ba-4d	0.0000	0.5000	0.2500	Ba(4d)-O_1(4e)	2.9853
Ca-2a	0.0000	0.0000	0.0000	Ba(4d)-O_2(8h)	2.7541
Mo-2b	0.5000	0.5000	0.0000	Ba(4d)-O_2(8h)	3.2934
O_1-4e	0.0000	0.0000	0.2772	Ca(2a)-$O_{1\text{-}2}$(4e-8h)	2.3735
O_2-8h	0.2322	0.3242	0.0000	Mo(2b)-$O_{1\text{-}2}$(4e-8h)	1.9070

Bond angles Ca–O_2–Mo: 158.9°; Tilt angle CaO_6: 9.395°; Tilt angle MoO_6: 11.723.°

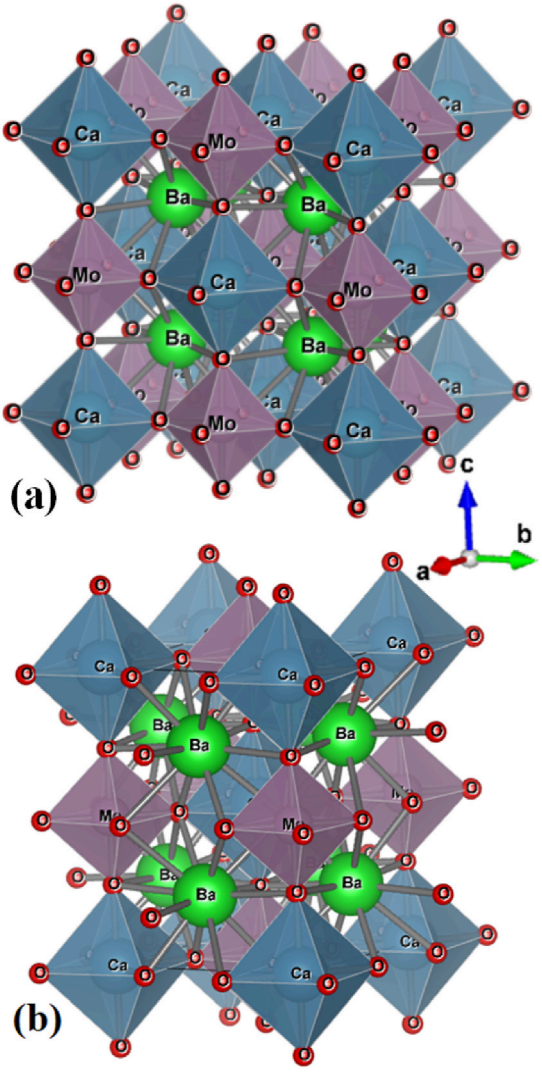

Fig. 1. Crystal structure of the double perovskite Ba_2CaMoO_6 in the cubic (a) and tetragonal (b) crystallographic phases.

effect on the octahedra of the tetragonal cell is evident in the Ca–*O*–Mo bond angles which have values of 158.9° instead of the 180.0° expected for the cubic cell.

3.2. Phononic frequencies

Since the difference between the minimum energies of the two structural phases was extremely small (65 meV), the term $-\left(\frac{\partial U}{\partial V}\right)_S V$, where $\left(\frac{\partial U}{\partial V}\right)_S$ is the pressure *P*, *U* is the total internal energy, *V* is the volume and *S* represents the entropy, was added to calculate the enthalpy of each of the systems, resulting in the result presented in Fig. 2, where a greater stability for the tetragonal phase can be appreciated, as well as a probable phase transition between the two structures when a pressure of 0.06 GPa is applied. In general, crystalline materials can exhibit phase transitions when changing temperature and pressure. The phase with a specified crystalline structure can exist in a stable state within a certain range of temperature and pressure, changing phase in critical value. Such stability in thermodynamic conditions is called phase stability. Both phase stability and intrinsic chemical instability under certain thermodynamic conditions can be predicted by determining the entropy through phonon calculations [25].

The Gibbs free energy of a compound as a function of temperature T and pressure P is given as

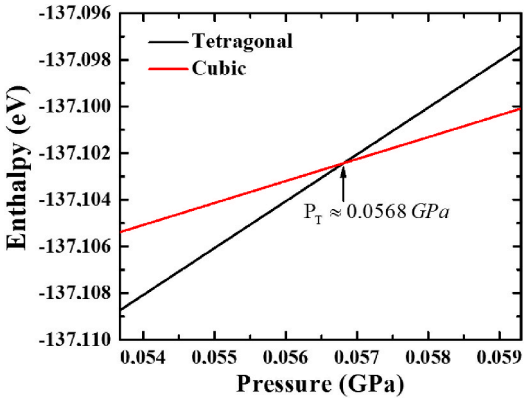

Fig. 2. Enthalpy as a function of pressure calculated for the Ba_2CaMoO_6 double perovskite in the tetragonal and cubic structural phases.

$$G(T,P) = F(T,V) + PV, \tag{3}$$

where F(T,V) is the Helmholtz free energy as a function of temperature and volume V.

For the PV term, the total energies are calculated by varying the unit cell volume, fitting the empirical equation of state of a solid [26] to obtain the function E(V), and then the pressure is estimated by performing the differentiation $P = -(\partial E/\partial V)T$ [27]. Within the adiabatic approximation, F(T,V) can be separated into ionic and electronic vibrational contributions [28,29],

$$F(T,V) = F_{vib}(T,V) + F_{elec}(T,V) \simeq F_{vib}(T,V) + E(T=0\,K,V) \tag{4}$$

In the Helmholtz electronic free energy term, $F_{elec}(T,V) = E(T=0\,K, V) - TS_{elec}$, the TS_{elec} term is ignored because the effect of electronic temperature is negligible for nonmetallic systems in the vicinity of room temperature [30]. Thus, within the quasi-harmonic approximation (QHA), the ionic term F_{vib} can be calculated as follows [27,29].

$$F_{vib}(T,V) = 3Mk_BT \int_0^{\omega L} Ln\left\{2\,sinh\left[\frac{h\omega(V)}{2k_BT}\right]\right\} g(\omega)d\omega \tag{5}$$

where $\omega(V)$ is the phonon frequency as a function of volume, *M* is the atomic mass, $g(\omega)$ is the normalized density of phonon states and ωL is the maximum of the phonon frequencies. The stability can be estimated by the Gibbs free energy difference between the two phases.

It is crucial to obtain an accurate picture of phonon scattering in perovskites to understand material processes such as ionic transport and charge carrier recombination and scattering, as well as material stabilities. Phonon scattering is computationally accessible through cell dynamics calculations, where the dynamic matrix is constructed through the Hessian matrix as the second derivatives of the total energy with respect to the atomic displacements that can be obtained directly from DFT calculations. The Hessian matrix (or interatomic force constant) can be calculated in real space by performing force calculations on a series of symmetry-inequivalent displaced structures with the use of a supercell [31,32] or in the reciprocal space using perturbation theory (DFPT) [28]. Diagonalizing the dynamic matrix yields a set of eigenvectors (phonon modes) and eigenvalues (phonon frequencies) [25].

Fig. 3 shows the calculated phonon dispersions for the cubic and tetragonal phases of the double perovskite Ba_2CaMoO_6.

The phonon frequencies of the vibrational spectrum for the cubic phase at Γ evidence a negative frequency, confirming its unstable character. For the tetragonal phase, no negative components are evident, reaffirming its stability.

The stability of the tetragonal phase is corroborated in Fig. 4, where the specific heat at constant volume as a function of temperature is presented, also showing the occurrence of a phase transition to a cubic

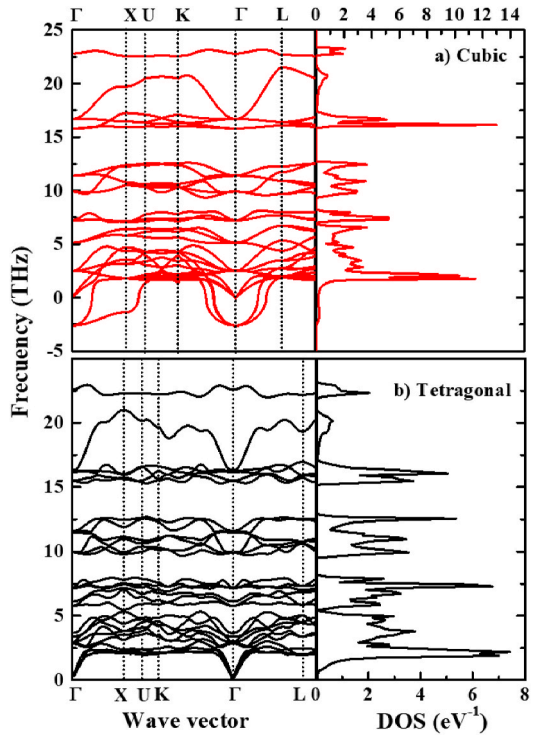

Fig. 3. Calculated phonon frequencies for the (a) cubic and (b) tetragonal crystallographic phases of the complex perovskite Ba_2CaMoO_6.

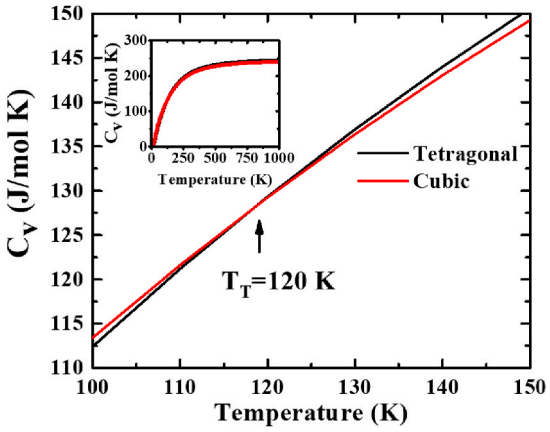

Fig. 4. Dependence of the specific heat at constant volume on temperature for the tetragonal and cubic phases of the double perovskite Ba_2CaMoO_6. The inset corresponds to the complete specific heat curve calculated for the Fm $\bar{3}$ m and *I4/m* space groups.

structure at T = 120 K.

Experimental reports through low-temperature X-ray synchrotron, neutron diffraction and differential scanning calorimetry reveal that a phase transition between a tetragonal structure at low temperatures and a cubic structure at high temperatures takes place at T = 200 K [33]. These theoretical results are supported by experimental vibrational spectroscopy measurements reported for frequencies in the infrared region related to Mo–O stretching (octahedral deformations of MoO_6) [34], and Raman frequencies corresponding to the deviation from the Oh symmetry presented in the cubic structure, as well as the vibration of oxygen in the octahedral coordination [34,35].

3.3. Optical properties

In order to discuss the differences between the spectra corresponding to the two structures under analysis, the linear optical properties were calculated from the frequency-dependent complex dielectric function ε(ω). The behaviour of the material when subjected to electromagnetic radiation is represented by

$$\varepsilon(\omega) = \varepsilon_1(\omega) + i\varepsilon_2(\omega) \tag{6}$$

where ω is the photon frequency and $\varepsilon_1(\omega)$ and $\varepsilon_2(\omega)$ are the real and imaginary parts of the dielectric function respectively. The real part provides information about the range of the energy stored in the Ba_2CaMoO_6 double perovskite and the imaginary part of the dielectric function provides the loss of the material energy due to photon absorption.

Fig. 5 shows the ε_1 and ε_2 curves for the cubic and tetragonal structures. In both cases the real part ε_1 show their first two maxima at 2.8 eV and 3.4 eV, but for the case of the cubic phase between 7 eV and 12 eV it is observed that $\varepsilon_1<0$, indicating that the light does not propagate through the material in that range of energies, while for the tetragonal case such effect is observed between 8 and 11 eV.

On the other hand, the values of the static dielectric constant $\varepsilon_1(0)$ are 4.4 and 5.5 for the cubic and tetragonal phase, respectively. These values are comparable with those reported for other double perovskite-like compounds such as Sr_2NiTeO_6 [36], $Cs_2AgBiBr_6$ [37], Cs_2ScTlI_6 [38] and Cs_2BiCuI_6 [39]. The imaginary part ε_2, which includes inter/-intra band contributions, shows the first peak at 3.7 and 3.6 eV for the cubic and tetragonal cases, respectively, which may be related to electronic transitions from 4d-Mo to 2p-O states at the conduction band and valence band. Furthermore, at energy values greater than 30 eV, ε_2 tends to zero, indicating that the surface of the material does not interact with the incident electromagnetic radiation.

Frequency-dependent linear optical spectra, as the refractive index $n(\omega)$, are key optical parameters for the design of optical connections and optical devices, which can be calculated from the real and imaginary parts of the dielectric function $\varepsilon_1(\omega)$ and $\varepsilon_2(\omega)$ [40],

$$n(\omega) = \left[\frac{\sqrt{\varepsilon_1^2+\varepsilon_2^2}+\varepsilon_1}{2}\right]^{\frac{1}{2}}, \tag{7}$$

Fig. 6 shows the values of refractive index $n(\omega)$ for Ba_2CaMoO_6 double perovskite in the tetragonal and cubic phases, which are key optical parameters for the design of optical junctions and devices.

The refractive index for this material under incident energy starts from 3.33 for the tetragonal and 3.5 for the cubic phase, reaching a maximum value close to 3.75 eV. This value is very close to the index

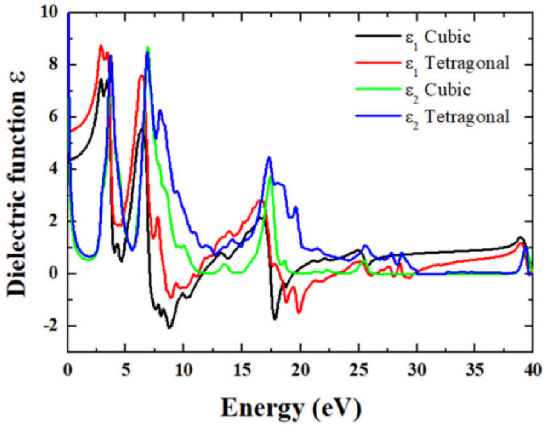

Fig. 5. Real and imaginary contributions to the dielectric function for the cubic and tetragonal structures.

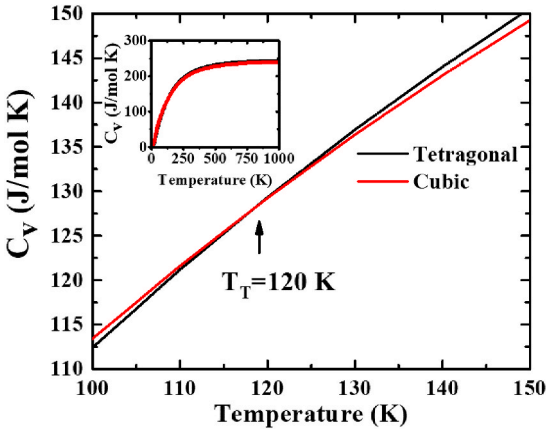

Fig. 6. Characteristic refractive index calculated for the tetragonal and cubic phases of the Ba_2CaMoO_6 material.

measured in semiconductor materials such as GaAs [41] and perovskite-type materials classifiable as very good semiconductors [42].

The absorption coefficient $\alpha(\omega)$, which represents the absorption capacity of any material subjected to electromagnetic radiation, is calculated as

$$\alpha(\omega) = \frac{\sqrt{2\omega}}{c}\left[\sqrt{\varepsilon_1^2 + \varepsilon_2^2} - \varepsilon_1\right]^{\frac{1}{2}} \tag{8}$$

Fig. 7 shows the variation of the absorption coefficient α(ω) due to the change in photon energy for double perovskite Ba_2CaMoO_6 in the tetragonal and cubic phases. In general terms, it can be observed that the absorption results for the two phases present similar behaviours with some exceptions at the energy levels of about 3.0 and 4.0 eV. The absorption coefficient for the cubic phase increases from 0.03 eV and for the tetragonal phase from 0.04 eV, reaching a maximum energy value of 3.75 eV for the two phases under study.

On the other hand, the energy loss function $L(\omega)$ of electrons is an important characteristic of materials that correlates with the scattering of high energy electrons from the material under analysis. This property is calculated by means of the following relation

$$L(\omega) = \frac{\varepsilon_2}{\varepsilon_1^2 + \varepsilon_2^2} \tag{9}$$

The energy loss function L(ω) of electrons of double perovskite Ba_2CaMoO_6 in the tetragonal and cubic phases is shown in Fig. 8, this function plays a very important role related to the high energy electron

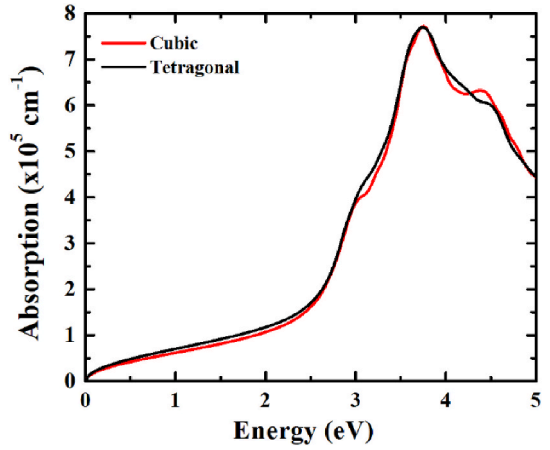

Fig. 7. Absorption spectra in the Ba_2CaMoO_6 double perovskite calculated for the cubic and tetragonal phases.

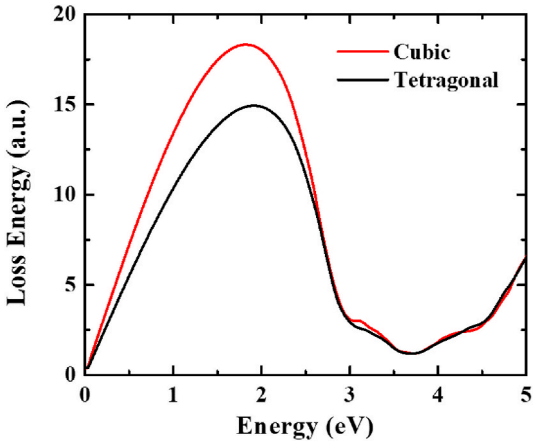

Fig. 8. Energy loss function in Ba_2CaMoO_6 double perovskite for the cubic and tetragonal phases.

scattering of the materials. That is, the peaks that exist in the electron energy loss function represent the plasma frequency also known as the resonance frequency. In any given material, above the resonance frequency, the material behaves as a dielectric and below this limiting value; the material behaves as a metal. For the energy range in Fig. 8, the highest peak appears in the energy range between 1.5 and 2.0 eV for the cubic and tetragonal phases.

At last, the reflectivity $R(\omega)$ that measures the ratio of the amplitude of reflected energy to the amplitude of incident energy is given by

$$R(\omega) = \frac{(n-1)^2 + k^2}{(n+1)^2 + k^2} \tag{10}$$

Fig. 9 shows the variation of the reflectivity calculated for the double perovskite Ba_2CaMoO_6 in the tetragonal and cubic phases, with photon energy up to 5 eV.

The reflectivity spectrum starts at 0.56 and 0.57 for the tetragonal and cubic phases respectively, with photon energy 0 eV. It then decreases to values close to 0.2 for a photon energy of 0.5 eV. Subsequently, it remains constant in an energy range from 0.5 to 2.6 eV, increasing to 0.39 for an energy range between 3.5 and 4.0 eV in an identical behaviour for both phases studied.

3.4. Electronic structure

The calculated band structure along the chosen high symmetry points is exemplified in Fig. 10 for the material Ba_2CaMoO_6 in the

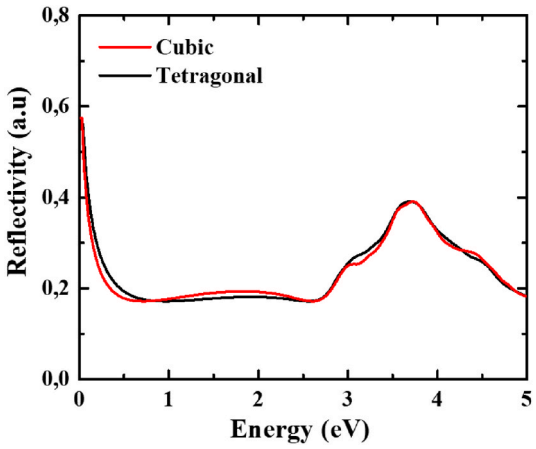

Fig. 9. Reflectivity behaviour for Ba_2CaMoO_6 material in the cubic and tetragonal phases.

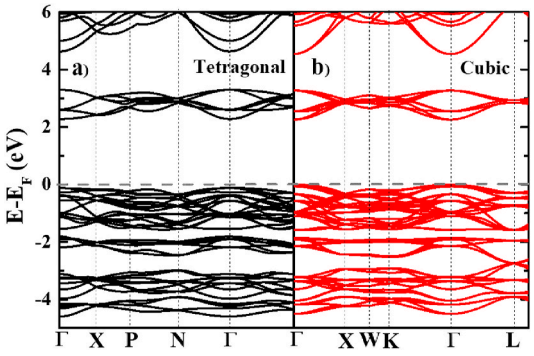

Fig. 10. Calculated electronic band structure for the tetragonal (a) and cubic (b) crystallographic phases in the Ba_2CaMoO_6 perovskite-like material.

tetragonal and cubic phases. A first observation allows to establish the occurrence of direct gap for the two phases, with semiconducting behavior, since, right at the fermi level, a band gap $E_g^T = 2.397$ eV is evidenced for the tetragonal structure and $E_g^C = 2.258$ eV for the cubic structure.

Additionally, in both the valence and conduction bands, close to the Fermi level denoted by $E_F = 0$ eV, a great similarity in the distribution of the electronic bands is evident. Meanwhile, a sharper observation shows that in the cubic phase the bands are more overlapped in both the valence and conduction bands than for the tetragonal phase. In order to observe the electronic distribution for the two structural phases under analysis, the density of electronic states shown in Fig. 11 was calculated, where the contributions of the Ba-*d* and d-Mo-*d* electrons, as well as the O-*p* electrons in the energetic vicinity of the Fermi level are displayed.

Fig. 11 shows that in the valence band, far from the Fermi level (-5.0 eV $< E < -3.0$ eV) the largest contributions correspond to O-*p* electrons, with a smaller participation of the d orbitals of Mo, while near the Fermi level (-3 eV $< E < 0$ eV) the O-p electrons are in the majority. On the other hand, in the conduction band, above a bandgap $E_g^T = 2.40$ eV for the tetragonal phase and $E_g^C = 2.26$ eV for the cubic, the electrons that contribute most are the *d* and *p* electrons of the Mo and O elements. Far and above E_F, in the 5.0 eV $< E <$ 7.0 eV regime, there are available *d* and *p* states of the Ba, Mo and O atoms, in that order of contribution.

4. Conclusions

The properties of the structural ground state, the dynamic cell and the optical properties of the double perovskite Ba_2CaMoO_6 have been investigated theoretically. The stability between the tetragonal and cubic phases has been evaluated. The results obtained show that the most stable phase is the tetragonal one, which is in agreement with the experimental results. The electronic properties of the examined compound show that Ba_2CaMoO_6 is semiconducting in nature with a wide direct bandgap with an energy of 2.40 eV for the tetragonal structure and 2.26 eV for the cubic structure. In addition, the optical properties of the double perovskite Ba_2CaMoO_6 have also been considered. The calculated optical properties of this compound take place between the ultraviolet and visible region of optical radiations and, therefore, we can suggest that the double perovskite Ba_2CaMoO_6 can be an alternative material for use in photodetectors, light emitters and power electronics applications.

CRediT author statement

C.E. Deluque Toro: He was responsible for writing the code as part of the direction of H.H. V.E. Vergara's doctoral thesis. V.E. Vergara: PhD. student who participated in the calculation of the density of electronic states. A.V. Gil Rebaza: Supervised the calculation of optical properties. D.A. Landínez Téllez: He participated in the interpretation of results. J. Roa-Rojas, corresponding author: Responsible for project management, interpretation of results and drafting of the manuscript.

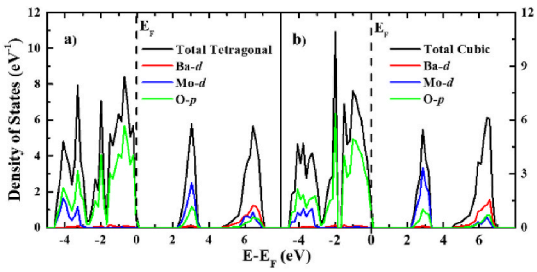

Fig. 11. Density of total and partial and total states of the double perovskite Ba_2CaMoO_6 in the tetragonal (a) and cubic (b) phases.

Declaration of competing interest

The authors declare that they have no known competing financial interests or personal relationships that could have appeared to influence the work reported in this paper.

Data availability

https://data.mendeley.com/datasets/brj6zwb4r9.

Acknowledgements

This work was partially supported by the División de Investigación y Extensión (DIEB, Hermes code 57456) of the Universidad Nacional de Colombia (Bogotá) and Fonciencias of the Universidad del Magdalena.

References

[1] S. Vasala, M. Karppinen, Progr. Solid State Chem. 43 (2015) 1–36.
[2] M.W. Lufaso, P.M. Woodward, Acta Cryst. B 57 (2001) 725–738.
[3] X.A. Velásquez Moya, R. Cardona, J.I. Villa Hernández, D.A. Landínez Téllez, J. Roa-Rojas, J. Electr. Mater. 47 (2018) 3421–3429.
[4] D.Y. Chen, F.Z. Chien, D.C. Ling, J.L. Tseng, S.R. Sheen, M.J. Wang, M.K. Wu, Phys. C Supercond. 282–287 (1997) 73–76.
[5] T. Maiti, M. Saxena, P. Roy, J. Mater. Res. 34 (2019) 107–125.
[6] T. Kise, T. Ogasawara, M. Ashida, Y. Tomioka, Y. Tokura, M. Kuwata-Gonokami, Phys. Rev. Lett. 85 (2000), 1986–1989.
[7] M. Bonilla, D.A. Landínez Téllez, J.A. Rodríguez, J.A. Aguiar, J. Roa-Rojas, J. Magn. Magn Mater. 320 (2008) e397–e399.
[8] V.R. Estrada Contreras, C.E. Alarcón Suesca, C.E. Deluque Toro, D.A. Landínez Téllez, J. Roa-Rojas, Ceram. Internat. 47 (2021) 14408–14417.
[9] J.A. Jaramillo Palacio, K.A. Muñoz Pulido, J. Arbey Rodríguez, D.A. Landínez Téllez, J. Roa-Rojas, J. Adv. Dielect. 11 (2021), 2140003.
[10] C.E. Deluque Toro, K.A. Muñoz Pulido, J. Arbey Rodríguez, D.A. Landínez Téllez, J. Roa-Rojas, J. Low Temp. Phys. 206 (2022) 269.
[11] M.P. Singh, K.D. Truong, S. Jandl, P. Fournier, J. Appl. Phys. 107 (2010), 09D917.
[12] N. Kumar, G. Khurana, R.S. Katiyar, A. Gaur, R. Kotnala, Double perovskite Sr_2FeMoO_6: a potential candidate for room temperature magnetoresistance device applications, in: Magnetic Sensors - Development Trends and Applications, IntechOpen, London, United Kingdom, 2017 (Online).
[13] I.D. Brown, Chem. Rev. 109 (2009) 6858–6919.
[14] I. Yamada, A. Takamatsu, H. Ikeno, Sci. Technol. Adv. Mater. 19 (2018) 101–107.
[15] H.W. Eng, P.W. Barnes, B.M. Auer, P.M. Woodward, J. Solid State Chem. 175 (2003) 94–109.
[16] C. Tablero, J. Alloys Compd. 639 (2015) 203–209.
[17] Loi T. Nguyen, Robert J. Cava, Allyson M. Fry-Petit, J. Solid State Chem. 277 (2019) 415–421.
[18] S. Faiza-Rubab, S. Naseem, S. M Alay-e-Abbas, M. Zulfiqar Y. Zhao, S. Nazir, Phys. Chem. Chem. Phys. 23 (2021) 19472–19481.
[19] G. Kresse, J. Joubert, Phys. Rev. B 59 (1999) 1758–1775.
[20] H.J. Monkhorst, J.D. Pack, Phys. Rev. B 13 (1976) 5188–5192.
[21] J.P. Perdew, Y. Wang, Phys. Rev. B 45 (1992) 13244–13249.
[22] A. Togo, F. Oba, I. Tanaka, Phys. Rev. B 78 (2008), 134106.
[23] C.E. Deluque Toro, A.S. Mosquera Polo, A.V. Gil Rebaza, D.A. Landínez Téllez, J Roa-Rojas, J. Low Temp. Phys. 192 (2018) 265–285.
[24] F.D. Murnaghan, Proc. Natl. Acad. Sci. 30 (1944) 244.
[25] K.T. Butler, A. Walsh, A.K. Cheetham, G. Kieslich, Chem. Sci. 7 (2016) 6316–6324.
[26] F. Birch, Phys. Rev. 71 (1947) 809–824.
[27] C.-J. Yu, G.-C. Ri, U.-G. Jong, Y.-G. Choe, S.-J. Cha, Physica B 434 (2014) 185–193.

[28] S. Baroni, S. de Gironcoli, A. Dal Corso, P. Giannozzi, Rev. Mod. Phys. 73 (2001) 515–562.
[29] B. Grabowski, T. Hickel J. Neugebauer, Phys. Rev. B 76 (2007), 024309.
[30] L. Landau, E. Lifschitz, Electrodynamics of Continuous Media, Pergamon), Oxford, 1960.
[31] K. Parlinski, Z.Q. Li, Y. Kawazoe, Phys. Rev. Lett. 78 (1997) 4063.
[32] L. Chaput, A. Togo, I. Tanaka, G. Hug, Phys. Rev. B 84 (2011), 094302.
[33] L.T. Nguyen, R.J. Cava, A.M. Fry-Petit, J. Solid State Chem. 277 (2019) 415–421.
[34] G. Blasse, J. Inorg. Nucl. Chem. 37 (1975) 1347–1351.
[35] L. Zhang, P. Han, Y. Han, Z. Lu, H. Yang, L. Wang, Q. Zhang, J. Alloys Compd. 558 (2013) 229–235.
[36] F.I.H. Alias, M.H. Ridzwan, M.K. Yaakob, C.W. Loy, Z. Mohamed, J. Mater. Res. Technol. 18 (2022) 1623–1630.
[37] N.H. Alotaibi, G.M. Mustafa, N.A. Kattan, Q. Mahmood, H. Albalawi, M. Morsi, H. H. Somaily, M.A. Hafez, H.I. Mahmoud, M.A. Amin, J. Sol. State Chem. 313 (2022), 123353.
[38] N. Erum, J. Ahmad, M.A. Iqbal, M. Ramzan, Opt. Quantum Electron 55 (2023) 337.
[39] M. Roknuzzaman, C. Zhang, K. Ostrikov, A. Du, H. Wang, L. Wang, T. Tesfamichael, Sci. Rep. 9 (2019) 718.
[40] Y.H.R. Chang, T.L. Yoon, T. L Lim, P.W. Koh, M.H. Tuh, J. Alloys Compd. 779 (2019) 497.
[41] V. Bardinal, R. Legros, C. Fontaine, Appl. Phys. Lett. 67 (1995) 244–246.
[42] J.K. Singh, S.K. Mandal, G. Banerjee, J. Mater. Res. 36 (2021) 1773–1793.